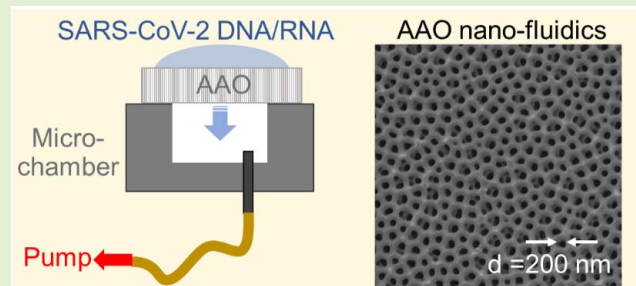


Surface Functionalized Anodic Aluminum Oxide Membrane for Opto-Nanofluidic SARS-CoV-2 Genomic Target Detection

Megan Makela¹, Zhihai Lin¹, and Pao Tai Lin¹

Abstract—An ultra-thin and highly sensitive SARS-CoV-2 detection platform was demonstrated using a nano-porous anodic aluminum oxide (AAO) membrane. The membrane surface was functionalized to enable efficient trapping and identification of SARS-CoV-2 genomic targets through DNA-DNA and DNA-RNA hybridization. To immobilize the probe oligonucleotides on the AAO membrane, the pore surface was first coated with the linking reagents, 3-aminopropyltrimethoxysilane (APTMS) and glutaraldehyde (GA), by a compact vacuum infiltration module. After that, complementary target oligos with fluorescent modifier was pulled and infiltrated into the nano-fluidic channels formed by the AAO pores. The fluorescent signal applying the AAO membrane sensors was two orders stronger than a flat glass template. In addition, the dependence between the nano-pore size and the fluorescent intensity was evaluated. The optimized pore diameter d is 200 nm, which can accommodate the assembled oligonucleotide and aminosilane layers without blocking the AAO nano-fluidic channels. Our DNA functionalized membrane sensor is an accurate and high throughput platform supporting rapid virus tests, which is critical for population-wide diagnostic applications result in a page being rejected by search engines.

Index Terms—AAO, biosensor, COVID-19, DNA, nanoporous.



I. INTRODUCTION

FROM the first incidence in Wuhan, China in late 2019 to the official declaration of a pandemic by the World Health Organization (WHO) less than four months later [1], [2], the novel coronavirus disease 2019 (COVID-19) outbreak has become one of the most critical public health challenges in recent memory. To date, more than 95 million cases and 2.0 million deaths have been reported worldwide [3]. The rapid spread of the underlying severe acute respiratory syndrome

coronavirus 2 (SARS-CoV-2) has been attributed to factors such as its airborne routes of transmission,[4] long incubation period and contagious times [5], and virulence [6]. The nature of non-specific symptoms and a large number of subclinical infections hinder the identification of cases causing unnoticeable spread of the virus [7]. Hence, strategies for controlling transmission have focused heavily on diagnostics, particularly the implementation of rapid and reliable testing methods [8]. One of the standard viral diagnostic test methods is based on reverse-transcription polymerase chain reaction (RT-PCR) that detects and amplifies specific target sequences of the viral nucleic acids. PCR kits for the SARS-CoV-2 virus have been commercially developed and distributed [9]. Nevertheless, the collection-to-result time for PCR tests can take days because the analyses need to be performed by trained technicians at a centralized laboratory. Current efforts have been directed toward decentralization of laboratory testing and the development of point-of-care (PoC) technologies that provide accurate results at the point of sample collection [10]. The preponderance of PoC diagnostic tests developed for COVID-19 are immunoassays, which typically take the format of lateral flow assays (LFAs) [11], [12]. Most LFAs are designed to detect antibodies, utilizing colloidal gold immunochromatography with patient blood or serum samples. These tests are extremely rapid, typically taking less than 15 minutes to produce a

Manuscript received August 1, 2021; accepted August 7, 2021. Date of publication August 31, 2021; date of current version October 18, 2021. This work was supported in part by the NSF Precise Advanced Technologies and Health Systems for Underserved Populations (PATHS-UP) Engineering Research Center under Grant 1648451, in part by NIH under Grant GM132705-02, and in part by Texas A&M University Presidential X-Grant. The associate editor coordinating the review of this article and approving it for publication was Prof. Chih-Ting Lin. (Corresponding author: Pao Tai Lin.)

Megan Makela is with the Center for Remote Health Technologies and Systems, Department of Materials Science and Engineering, Texas A&M University, College Station, TX 77843 USA.

Zhihai Lin is with the Department of Electrical and Computer Engineering, Texas A&M University, College Station, TX 77843 USA.

Pao Tai Lin is with the Departments of Electrical and Computer Engineering and Materials Science and Engineering, Texas A&M University, College Station, TX 77843 USA, and also with the Center for Remote Health Technologies and Systems, Texas A&M University, College Station, TX 77843 USA (e-mail: paolin@ece.tamu.edu).

Digital Object Identifier 10.1109/JSEN.2021.3109022

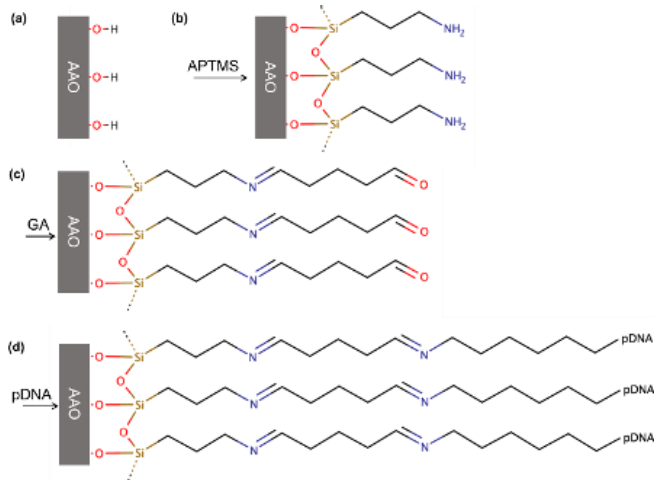


Fig. 1. The processes of surface modification and pDNA immobilization. (a) Functionalization of the AAO nano-pore surface with hydroxyl groups, (b) salinization with APTMS, (c) coating with the GA layer, and (d) immobilization with the pDNA oligonucleotides.

result, simple to administer and inexpensive to manufacture. However, these systems have limitations including poorer sensitivity and specificity than laboratory tests and inability to detect early infections [13], [14]. LFAs designed for antigen detection, the presence of viral protein in respiratory samples, is more effective for diagnosis of acute infection, but suffer from issues with false negatives in asymptomatic patients or those with low viral load [15], [16].

Among various viral diagnostic platforms, optofluidic biosensors can be miniaturized as chip-scale devices providing advantages of convenience and rapid testing. Yet, challenges remain in tracing low concentration genetic targets since it requires both high sensitivity and selectivity. An attractive approach to improve detection sensitivity is to implement nano-porous structures that possess a large surface area, such as an AAO membrane or porous silicon (p-Si). A biosensor with extensive surface area creates additional binding sites to immobilize bioreceptor molecules, thus capable of trapping a large amount of target molecules. The increased interaction at the interface between the sensor and analyte not only improves the detection sensitivity, but also reduces the device footprint. For instance, metallic or metal-coated nano-porous membranes have been utilized in electrochemical biosensors to detect DNA [17]–[19], protein [20], and enzymes [21], [22]. For the same reason, dielectric nano-porous media have been applied in numerous optofluidic sensing devices, such as single-layer p-Si to detect binding reactions of small organic molecules, DNA, and proteins through reflectance spectroscopy [23]. More complex devices are double-layer p-Si reflective interferometric sensors [24], multi-layered Bragg p-Si immunosensors [25], and porous micro-cavities for whole blood IgG detection [26].

Among various nano-porous media, AAO membrane is of particular interest to optofluidic biosensing because of its easy fabrication and high compatibility with biomaterials [27], [28]. A typical AAO membrane is a high density array consisting of hexagonally close-packed Al_2O_3 cells, each with a central cylindrical pore. It is formed through reproducible electrochemical self-assembly, a process that can precise controls

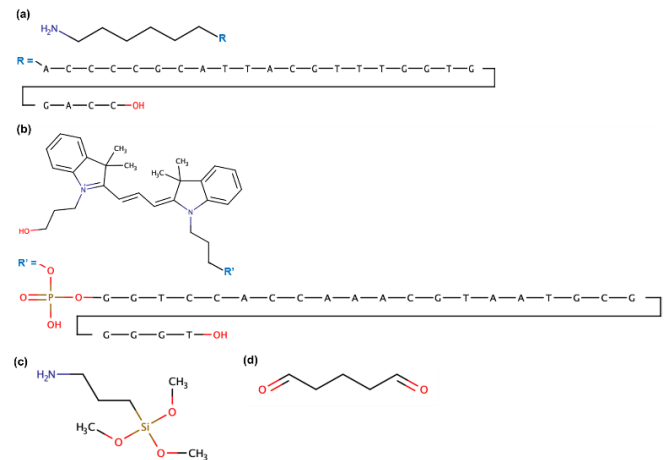


Fig. 2. Chemical structure of the oligonucleotides and the surface functionalization molecules. (a) The sequence and modifier chemistry of the pDNA molecule. (b) The Cy3-modified tDNA. RNA target is identical to (b) except that the tyrosine (T) is replaced by uracil (U). (c) The organosilane APTMS (d) The linker molecule GA.

characteristic structural parameters such as pore size and density by adjusting the anodization conditions. Compared to other complicated nano-patterning techniques like electron-beam lithography, the fabrication of AAO is scalable, simple, and cost-effective. Additionally, in the presence of hydroxyl groups on the porous AAO surfaces, it can be chemically modified and then bonded with various receptor molecules, hence enabling specificity in genomic identification. AAO has been used in quartz crystal microbalance (QCM) device and integrated localized surface plasmon resonance (LSPR)/quartz crystal microbalance dissipation (QCM-D) to enhance their sensitivity [29], [30]. Improvement of detection limit and observation of biomolecular interactions have been demonstrated. Unlike metallic porous media and p-Si that are opaque in the visible or near infrared, the broad optical transparency of AAO makes it suitable for sensing application over a wide spectral region, including the typical fluorescence detection. Compared to the AAO assisted QCM sensor, our optical AAO sensor applies a non-contact detection method to avoid the noise caused by the metal contact in the QCM device. Unlike LSPR devices that requires a broadband light source to measure the shift of the plasmon resonance wavelength, our fluorescence based measurement only requires a single-wavelength light source that simplifies the experimental set-up. These advantages make our AAO membrane sensors an exceptional platform for the development of PoC diagnostic devices.

II. MATERIALS AND METHODS

Schematics of the sensor preparation and surface functionalization are illustrated in Fig. 1. The AAO membranes obtained from InRedox (Longmont, CO, USA) were fabricated by aluminum electrochemical anodization methods, using voltage and temperature to tune the resulting structural parameters [31]. The surface of AAO nano-pores was first functionalized by surface binding reagents, APTMS and GA, through the layer-by-layer coating approach. Next, the probe DNA (pDNA) was immobilized onto the nano-pores. The chemical structures of the pDNA, target oligonucleotides

TABLE I
PARAMETERS OF AAO TEMPLATES

Diameter	Thickness	Pore Diameter	Pore Density	Porosity
10 mm	50 μm	20 nm	$5 \times 10^{10} \text{ cm}^{-2}$	11 %
10 mm	100 μm	80 nm	$3 \times 10^9 \text{ cm}^{-2}$	15 %
10 mm	100 μm	160 nm	$8 \times 10^8 \text{ cm}^{-2}$	16 %
10 mm	100 μm	200 nm	$5 \times 10^8 \text{ cm}^{-2}$	16 %

The parameters of the nano-porous AAO membranes, including the template diameter and thickness, pore diameter, and corresponding pore density and porosity.

(tDNA, RNA), APTMS, and GA are drawn in Fig. 2 (a) - (d), respectively. During the vacuum infiltration process, a compact polydimethylsiloxane (PDMS) chamber was mounted onto the AAO membrane that ensured the surface of the nano-pores was fully wetted by the reagents. The created molecular binding sites were designed to trap a specific oligonucleotide RNA sequence from the SARS-CoV-2 virus nucleocapsid (N) gene, as well as a sequence-equivalent DNA molecule.

The pDNA with sequence (5' NH₂(CH₂)₆ - ACC CCG CAT TAC GTT TGG TGG ACC - 3'), the complementary tDNA analyte (5' Cy3 -GGT CCA CCA AAC GTA ATG CCG GGT - 3'), and the complementary RNA analyte (5' Cy3 - rGrGrU rCrCrA rCrCrA rArArC rGrUrA rArUrG rCrGrG rGrGrU - 3') were synthesized by Integrated DNA Technologies (IDT). This probe has been identified by the Centers for Disease Control and Prevention (CDC) for detection of the nucleocapsid (N) gene of the SARS-CoV-2 virus and used in the molecular assays for respiratory viral testing [32]. The oligo solutions were prepared with sterilized deionized (DI) water. APTMS and GA (50 wt% solution in water) were purchased from Sigma Aldrich (St. Louis, MO, USA). All other reagents and solvents were laboratory grade or better and used as received, unless otherwise stated.

A. Preparation of the AAO Membrane and Vacuum Infiltration System

Our DNA-DNA and DNA-RNA hybridization-based biosensors were fabricated by applying successive coatings of APTMS, GA, and pDNA onto the nano-porous surface of AAO membranes. The freestanding membranes are 50 and 100 μm thick templates with a 10 mm diameter. The nano-pore sizes range from 20 to 200 nm diameters. Table I summarizes the corresponding pore density and porosity for each template. In order to uniformly coat the nano-pore surface, a vacuum infiltration system was built to pull the reagent solutions thoroughly through the membrane. As shown in Fig. 3, a thin AAO template was placed on top of a PDMS chamber, where the outlet made by a hypodermic needle was connected to a 3 mL syringe with tubing. A syringe pump was used to pull a vacuum on the system and the PDMS chamber, thus drawing the analytes dropped on the template's top surface into the fluidic channels formed by the nano-pores. The vacuum infiltration process took only a few minutes, as the volume of material is small. The same volume of sample (10 μL) was used on each of the AAO templates and the reference glass substrate. Damage to the AAO during the vacuum infiltration process was prevented by using the precision syringe pump, where the withdrawal rate can be held constant. This allowed

the control of the linear force provided by the pump and maintained a low pressure in the syringe and chamber.

Viral target RNA from biological patient samples can be obtained using a commercially available spin-column based RNA isolation kit, such as the QIAamp Viral RNA kit, with sample pre-treatment dependent on the sample type [33]–[35]. Additionally, no-kit methods for RNA extraction have been demonstrated and could be used for isolation of RNA in a real application.

B. Immobilization of the Probe DNA

Immobilization of the DNA probes on the pore inner surface was achieved via silanization followed by a homobifunctional linker. A dry AAO template was first coated with 0.1% APTMS in ethanol solution using the vacuum infiltration module. The reaction of the aminosilane with the AAO involved hydrolysis and condensation that formed siloxane linkages, along with additional hydrogen bonding and electrostatic interactions. Additional alkoxy groups on the APTMS can react with neighboring aminosilane molecules to form a networked silica layer. Excess APTMS residue on top of the membrane was removed by an ethanol rinse. The membrane was then dried in air for an hour. Next, the nano-pores were rinsed with ethanol by vacuum pulling. The membrane was cured on a hot plate at 120 °C to complete the cross-linking, followed by another rinse in ethanol and dry in air. After the surface silanization, the same pulling and rinsing processes were repeated using 2.5% GA in water. The sample was then dried again in air for an hour. The APTMS-GA modified AAO membrane had an aldehyde functionality, which can react with the amine group of the pDNA and form a secondary amine linkage for immobilization. A 10 μM solution of the 5'-aminated pDNA was pulled into the AAO nano-pores using the syringe pumping system. The concentration of 10 μM was selected to be on the same order of magnitude as the probe DNA used in the conventional DNA microarray printing process, which uses a similar amine-reactive immobilization concept [36]. Subsequently, the membrane was rinsed with DI water and blown dry with air. The probe coated membrane was covered and incubated for an hour. Afterward, additional water was pulled through the nano-pores to clean its surface.

C. Detection of the Genomic Target Analytes

Detection of the DNA and RNA target analytes was performed by a DNA-DNA and DNA-RNA hybridization method, where 10 μL target solution was added onto the device surface. RNA can hybridize with a complementary single strand of DNA to form a heteroduplex by the same mechanism that complementary DNA strands form a duplex [37]. In the case of applying surface functionalized AAO membranes, the process was completed following the same vacuum pulling procedure as used in the previous immobilization steps. For the non-porous glass substrate, the 10 μL volume of tDNA and RNA were spotted directly on the glass surface using a micropipette. The substrate was covered and incubated at room temperature for 1 hour and the unhybridized genomic targets were subsequently rinsed away with sterilized DI water. After the hybridization step, all devices were placed into a black polystyrene well plate with coated side facing upward.

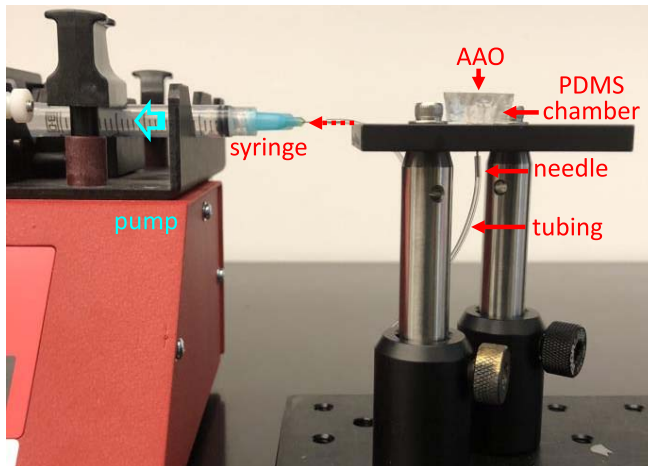


Fig. 3. A syringe pump used to pull vacuum on the system and draw liquid analytes, such as surface binding reagents, oligos, and rinses, into the AAO nano-pores. The AAO template was placed on top of a PDMS chamber, which was connected to a pump with tubing and a syringe outlet.

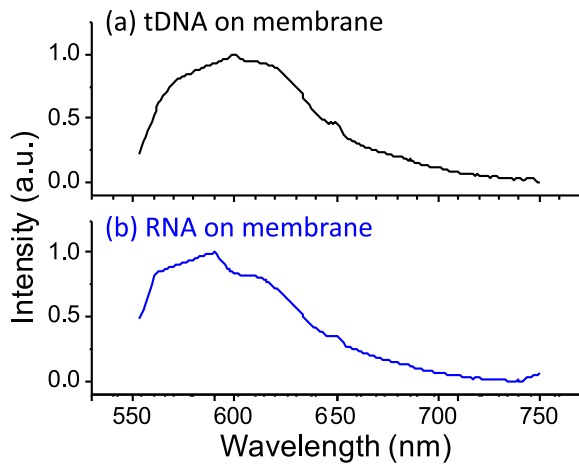


Fig. 4. Fluorescence spectra of the SARS-CoV-2 (a) tDNA and (b) RNA captured by the DNA functionalized membrane sensor in a AAO membrane with pore diameter $d = 200$ nm.

Following surface coating and capture steps, the devices were stored covered at room temperature for up to weeks between repeated measurements. The coated AAO is functional over the stability range of the DNA probe itself, including temperatures from room temperature to around 90°C and over a neutral pH range between 5 and 9. Absorption, top reflected fluorescence, and bottom transmitted fluorescence were measured using a Tecan Infinite M Nano⁺ Pro plate reader (Tecan, Männedorf, Switzerland). The excitation wavelength was 532 nm corresponding to a typical laser line used with the Cy3 fluorophore. Fluorescence spectra were obtained using a PTI-QuantaMaster spectrofluorometer (Photon Technology International, now HORIBA Scientific, Kyoto, Japan) with a Xe arc lamp. The wavelength of excitation was also 532 nm.

III. RESULTS AND DISCUSSION

A. Fluorescence Measurements and Sensitivity Enhancement

Fig. 4 (a) and (b) show the fluorescence spectra of the SARS-CoV-2 tDNA and RNA immobilized on the AAO

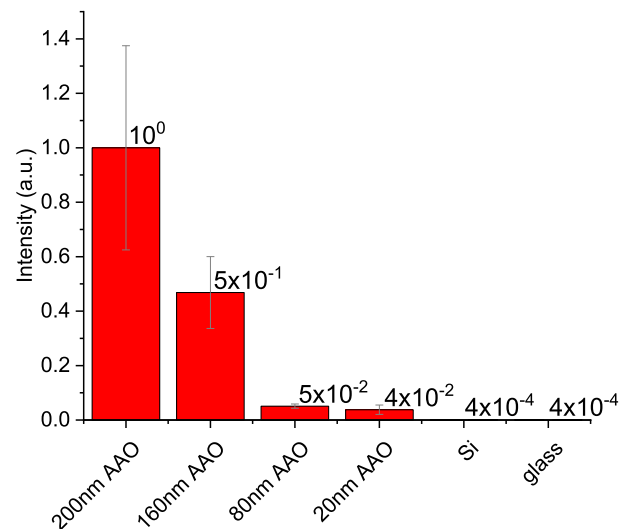


Fig. 5. Fluorescence intensity from the SARS-CoV-2 tDNA using the AAO membranes with $d = 20\text{--}200$ nm and a non-porous glass. Two orders of fluorescence enhancement was found from the $d = 200$ nm membrane. The large error in the higher fluorescence intensity was due to the saturation limit of the measurement system.

membranes, each normalized to their emission maximum respectively. For the tDNA, a strong fluorescent signal was observed from $\lambda = 550$ to 650 nm with a long tail extended to $\lambda = 750$ nm. Meanwhile, the RNA on membranes displayed a similar spectral profile, indicating our membrane sensors capable of detecting different genomic targets through oligo hybridization. Fig. 5 shows the comparison of fluorescence intensity from membranes with different AAO pore diameter d , where a strong correlation between d and the fluorescence intensity was found. Comparing to the tDNA on a glass template, the membrane with $d = 200$ nm showed two orders of fluorescence enhancement. The large error in the high fluorescence intensity values is due to its values near to the saturation limit of the measurement system. The significant increase of fluorescence is contributed by the large surface area from the nano-pores, since the trapping efficiency of the genomic targets is determined by the number of the pDNA binding sites and it is proportional to the available surface area. Computed from geometric methods, the $d = 200$ nm membrane has a substantial surface area of 247 cm^2 , while the same sized glass template is only 0.25 cm^2 . In addition to the large surface area from the AAO, its nanostructure also alternates the spatial emission mode of the fluorescence, thus increasing the optical signals [38], [39]. The optical interference caused by the AAO periodic nanostructure introduced an angle-dependent emission profile and strongly improved the fluorescence emission efficiency in the out-of-plane direction [40], [41].

It was also observed that the fluorescence intensity decreases with the pore size. The intensity from the $d = 160$ nm membrane is three times lower than the $d = 200$ nm, and $d = 80$ nm membrane is 20 times weaker. Nevertheless, the surface area of the $d = 160$ and $d = 80$ nm membranes are 1.3x and 2x larger than the $d = 200$ nm. The decrease of fluorescence intensity at a smaller d is due to the blockage of the nano-fluidic channels for the smaller

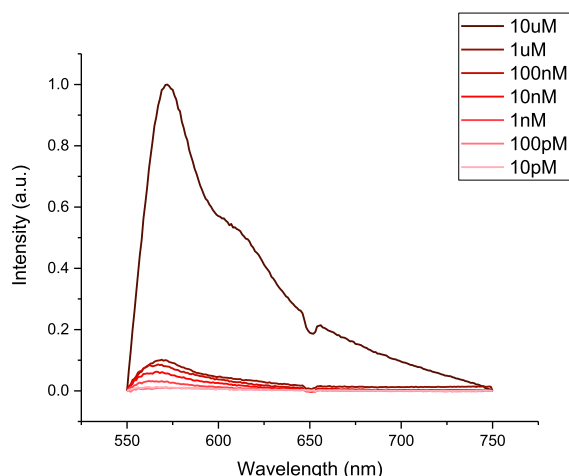


Fig. 6. Fluorescence spectra of the SARS-CoV-2 tDNA with decreasing concentrations of 10 μ M, 1 μ M, 100 nM, 10 nM, 1 nM, 100 pM, 10 pM sequence to the immobilized capture probe on $d = 200$ nm AAO templates.

AAO pores, since the pore size considerably decreased after the surface modification and probe immobilization processes. In addition, some APTMS molecules self-assembled and formed longer oligomers during the surface silanization. As such, the thickness of the AAO inner wall was increased by tens of nanometers for the membranes with $d < 100$ nm [42]–[45]. Moreover, the nanofluidic channels of the smaller AAO membranes provide increased fluid resistance compared to large pore diameters. As the coating materials and analyte DNA in small pore membranes face greater resistance during the same vacuum coating process, the coverage and uniformity of the surface coating may be reduced, also contributing to a lower signal intensity. Thus, of those tested devices, the ideal d for hybridization based oligos detection is the $d = 200$ nm membrane.

In addition to comparison of AAO and glass substrates, a concentration study was performed using the $d = 200$ nm pore size AAO that showed the highest enhancement of fluorescence signals. Fig. 6. presents the fluorescence spectrum for a range of target DNA concentrations: 10 μ M, 1 μ M, 100 nM, 10 nM, 1 nM, 100 pM, and 10 pM. A negative control, a Cy3-labeled DNA target that is non-complementary to the immobilized probe, was also coated on the AAO substrate at a concentration of 10 μ M. The fluorescence intensity from the non-hybridized DNA was found to be weaker than the comparable 10 μ M target DNA sample.

A linear detection range near three orders of magnitude was found, from 10 μ M to 10 nM concentrations of tDNA. The normalized maximum fluorescence intensity versus complementary target DNA concentration is plotted in Fig. 7., along with the fitted linear regression model. The limit of detection can be approximated from the signal-to-noise ratio of concentrations near the limit ($\text{SNR} \geq 3.0$) [46]. From the 10 pM sample, the noise bandwidth is about 0.002 a.u. with an overlapping signal of around 0.012 a.u., indicating that the AAO sensor is capable of detecting analyte in the picomolar to nanomolar range. Sensitivity is taken to be the slope of the fitted least squares regression model in the linear detection range, which is 9.5×10^4 a.u./M.

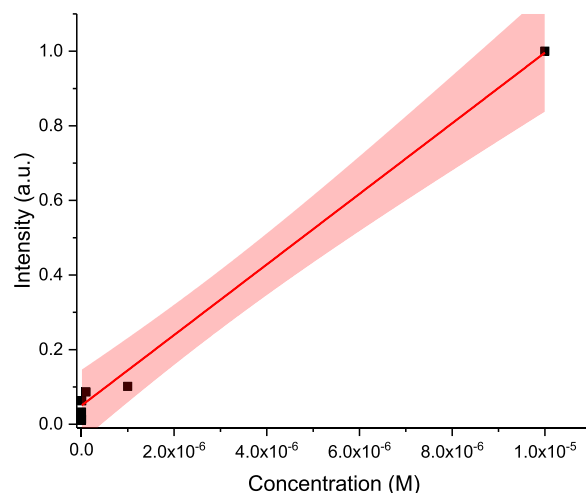


Fig. 7. Normalized maximum fluorescence intensity versus concentration of complementary target DNA from 10 μ M to 10 pM, shown with fitted linear regression model and confidence intervals. A linear detection range is found at the concentration between 10 μ M and 10 nM.

IV. CONCLUSION

A compact sensing device for detecting SARS-CoV-2 genomic material was demonstrated using a nano-porous AAO membrane. The pore surface was chemically modified by APTMS and linker molecule GA to immobilize the probe DNA oligonucleotides. The sensor was able to trap and identify SARS-CoV-2 genomic targets utilizing a DNA-DNA and DNA-RNA hybridization method. A two orders of magnitude fluorescence enhancement was achieved due to the large surface area created by the nano-porous structure. Additionally, an optimized pore diameter preventing the blockage of nanofluidic channels was found at $d = 200$ nm. The surface functionalized membrane device provides an accurate and miniaturized sensing component for the development of PoC viral diagnostics.

ACKNOWLEDGMENT

Characterization was performed at the Materials Characterization Facility (MCF) at Texas A&M University.

REFERENCES

- [1] N. Zhu *et al.*, “A novel coronavirus from patients with pneumonia in China, 2019,” *New Eng. J. Med.*, vol. 382, no. 8, pp. 727–733, Feb. 2020.
- [2] T. A. Ghebreyesus. (Mar. 2020). *WHO Director-General’s Opening Remarks at the Media Briefing on COVID-19*. World Health Organization. Accessed: Aug. 25, 2020. [Online]. Available: <https://www.who.int/dg/speeches/detail/who-director-general-s-opening-remarks-at-the-media-briefing-on-covid-19—11-march-2020>
- [3] E. Dong, H. Du, and L. Gardner, “An interactive web-based dashboard to track COVID-19 in real time,” *Lancet Infectious Diseases*, vol. 20, no. 5, pp. 533–534, 2020, doi: [10.1016/S1473-3099\(20\)30120-1](https://doi.org/10.1016/S1473-3099(20)30120-1).
- [4] Y.-H. Jin *et al.*, “A rapid advice guideline for the diagnosis and treatment of 2019 novel coronavirus (2019-nCoV) infected pneumonia (standard version),” *Mil. Med. Res.*, vol. 7, no. 1, pp. 1–23, Feb. 2020, doi: [10.1186/s40779-020-0233-6](https://doi.org/10.1186/s40779-020-0233-6).
- [5] X. Jiang, S. Rayner, and M. H. Luo, “Does SARS-CoV-2 has a longer incubation period than SARS and MERS?” *J. Med. Virol.*, vol. 92, no. 5, pp. 476–478, 2020, doi: [10.1002/jmv.25708](https://doi.org/10.1002/jmv.25708).
- [6] A. B. Gussow, N. Auslander, G. Faure, Y. I. Wolf, F. Zhang, and E. V. Koonin, “Genomic determinants of pathogenicity in SARS-CoV-2 and other human coronaviruses,” *Proc. Nat. Acad. Sci. USA*, vol. 117, no. 26, pp. 15193–15199, Jun. 2020, doi: [10.1073/pnas.2008176117](https://doi.org/10.1073/pnas.2008176117).

- [7] W. E. Wei, Z. Li, C. J. Chiew, S. E. Yong, M. P. Toh, and V. J. Lee, "Presymptomatic transmission of SARS-CoV-2—Singapore, January 23–March 16, 2020," *MMWR. Morbidity Mortality Weekly Rep.*, vol. 69, no. 14, pp. 411–415, Apr. 2020, doi: [10.15585/mmwr.mm6914e1](https://doi.org/10.15585/mmwr.mm6914e1).
- [8] F. Yu, L. Du, D. M. Ojcius, C. Pan, and S. Jiang, "Measures for diagnosing and treating infections by a novel coronavirus responsible for a pneumonia outbreak originating in Wuhan, China," *Microbes Infection*, vol. 22, no. 2, pp. 74–79, Mar. 2020, doi: [10.1016/j.micinf.2020.01.003](https://doi.org/10.1016/j.micinf.2020.01.003).
- [9] V. M. Corman *et al.*, "Detection of 2019 novel coronavirus (2019-nCoV) by real-time RT-PCR," *Eurosurveillance*, vol. 25, no. 3, Jan. 2020, Art. no. 2000045, doi: [10.2807/1560-7917.ES.2020.25.3.2000045](https://doi.org/10.2807/1560-7917.ES.2020.25.3.2000045).
- [10] B. Udugama *et al.*, "Diagnosing COVID-19: The disease and tools for detection," *ACS Nano*, vol. 14, no. 4, pp. 3822–3835, Apr. 2020, doi: [10.1021/acsnano.0c02624](https://doi.org/10.1021/acsnano.0c02624).
- [11] World Health Organization. (Apr. 8, 2020). *Advice on the Use of Point-of-Care Immunodiagnostic Tests for COVID-19: Scientific Brief, 8 April 2020*. WHO/2019-nCoV/Sci_Brief/POC_immunodiagnosics/2020.1. Accessed: Jul. 30, 2021. [Online]. Available: <https://apps.who.int/iris/handle/10665/331713>
- [12] K. Green, S. Graziadio, P. Turner, T. Fanshawe, and J. Allen, "Molecular and antibody point-of-care tests to support the screening, diagnosis and monitoring of COVID-19," Oxford COVID-19 Evidence Service Team, Centre Evidence-Based Med., Nuffield Dept. Primary Care Health Sci., Univ. Oxford, Oxford, U.K., Tech. Rep., 2020, p. 12.
- [13] B. Flower *et al.*, "Clinical and laboratory evaluation of SARS-CoV-2 lateral flow assays for use in a national COVID-19 seroprevalence survey," *Thorax*, vol. 75, no. 12, pp. 1082–1088, Dec. 2020, doi: [10.1136/thoraxjnl-2020-215732](https://doi.org/10.1136/thoraxjnl-2020-215732).
- [14] B. Ragnesola, D. Jin, C. C. Lamb, B. H. Shaz, C. D. Hillyer, and L. L. Luchsinger, "COVID19 antibody detection using lateral flow assay tests in a cohort of convalescent plasma donors," *BMC Res. Notes*, vol. 13, no. 1, p. 372, Aug. 2020, doi: [10.1186/s13104-020-05212-0](https://doi.org/10.1186/s13104-020-05212-0).
- [15] J. Dinnes *et al.*, "Rapid, point-of-care antigen and molecular-based tests for diagnosis of SARS-CoV-2 infection," *Cochrane Database Syst. Rev.*, vol. 8, Aug. 2020, Art. no. CD013705.
- [16] V. M. Corman *et al.*, "Comparison of seven commercial SARS-CoV-2 rapid point-of-care antigen tests: A single-centre laboratory evaluation study," *Lancet Microbe*, vol. 2, no. 7, pp. e311–e319, Jul. 2021, doi: [10.1016/S2666-5247\(21\)00056-2](https://doi.org/10.1016/S2666-5247(21)00056-2).
- [17] K. Hu, D. Lan, X. Li, and S. Zhang, "Electrochemical DNA biosensor based on nanoporous gold electrode and multifunctional encoded DNA–Au bio bar codes," *Anal. Chem.*, vol. 80, no. 23, pp. 9124–9130, Dec. 2008, doi: [10.1021/ac8017197](https://doi.org/10.1021/ac8017197).
- [18] M. Archer and P. M. Fauchet, "Electrical sensing of DNA hybridization in porous silicon layers," *Phys. Status Solidi A*, vol. 198, no. 2, pp. 503–507, Aug. 2003, doi: [10.1002/psa.200306641](https://doi.org/10.1002/psa.200306641).
- [19] J. Deng and C.-S. Toh, "Impedimetric DNA biosensor based on a nanoporous alumina membrane for the detection of the specific oligonucleotide sequence of dengue virus," *Sensors*, vol. 13, no. 6, pp. 7774–7785, Jun. 2013, doi: [10.3390/s130607774](https://doi.org/10.3390/s130607774).
- [20] S.-H. Yeom *et al.*, "Highly sensitive nano-porous lattice biosensor based on localized surface plasmon resonance and interference," *Opt. Exp.*, vol. 19, no. 23, pp. 22882–22891, Nov. 2011, doi: [10.1364/OE.19.022882](https://doi.org/10.1364/OE.19.022882).
- [21] R. R. K. Reddy, I. Basu, E. Bhattacharya, and A. Chadha, "Estimation of triglycerides by a porous silicon based potentiometric biosensor," *Curr. Appl. Phys.*, vol. 3, no. 2, pp. 155–161, Apr. 2003, doi: [10.1016/S1567-1739\(02\)00194-3](https://doi.org/10.1016/S1567-1739(02)00194-3).
- [22] M.-J. Song, D.-H. Yun, N.-K. Min, and S.-I. Hong, "Electrochemical biosensor array for liver diagnosis using silanization technique on nanoporous silicon electrode," *J. Biosci. Bioeng.*, vol. 103, no. 1, pp. 32–37, Jan. 2007, doi: [10.1263/jbb.103.32](https://doi.org/10.1263/jbb.103.32).
- [23] V. S.-Y. Lin, K. Moteshareh, K.-P. S. Dancil, M. J. Sailor, and M. R. Ghadiri, "A porous silicon-based optical interferometric biosensor," *Science*, vol. 278, no. 5339, pp. 840–843, Oct. 1997, doi: [10.1126/science.278.5339.840](https://doi.org/10.1126/science.278.5339.840).
- [24] C. Pacholski, M. Sartor, M. J. Sailor, F. Cumin, and G. M. Miskelly, "Biosensing using porous silicon double-layer interferometers: Reflective interferometric Fourier transform spectroscopy," *J. Amer. Chem. Soc.*, vol. 127, no. 33, pp. 11636–11645, Aug. 2005, doi: [10.1021/ja0511671](https://doi.org/10.1021/ja0511671).
- [25] X. Lv *et al.*, "Novel multilayered porous silicon-based immunosensor for determining hydroxysafflor yellow a," *Appl. Surf. Sci.*, vol. 257, no. 6, pp. 1906–1910, Jan. 2011, doi: [10.1016/j.apsusc.2010.09.024](https://doi.org/10.1016/j.apsusc.2010.09.024).
- [26] L. M. Bonanno and L. A. DeLouise, "Whole blood optical biosensor," *Biosens. Bioelectron.*, vol. 23, no. 3, pp. 444–448, Oct. 2007, doi: [10.1016/j.bios.2007.05.008](https://doi.org/10.1016/j.bios.2007.05.008).
- [27] T. Kumeria, A. Santos, and D. Losic, "Nanoporous anodic alumina platforms: Engineered surface chemistry and structure for optical sensing applications," *Sensors*, vol. 14, no. 7, pp. 11878–11918, Jul. 2014, doi: [10.3390/s140711878](https://doi.org/10.3390/s140711878).
- [28] A. Santos, T. Kumeria, and D. Losic, "Nanoporous anodic aluminum oxide for chemical sensing and biosensors," *TrAC Trends Anal. Chem.*, vol. 44, pp. 25–38, Mar. 2013, doi: [10.1016/j.trac.2012.11.007](https://doi.org/10.1016/j.trac.2012.11.007).
- [29] N. Asai, T. Shimizu, S. Shingubara, and T. Ito, "Fabrication of highly sensitive QCM sensor using AAO nanoholes and its application in biosensing," *Sens. Actuators B, Chem.*, vol. 276, pp. 534–539, Dec. 2018, doi: [10.1016/j.snb.2018.08.094](https://doi.org/10.1016/j.snb.2018.08.094).
- [30] N. Asai, N. Matsumoto, I. Yamashita, T. Shimizu, S. Shingubara, and T. Ito, "Detailed analysis of liposome adsorption and its rupture on the liquid-solid interface monitored by LSPR and QCM-D integrated sensor," *Sens. Bio-Sens. Res.*, vol. 32, Jun. 2021, Art. no. 100415, doi: [10.1016/j.sbsr.2021.100415](https://doi.org/10.1016/j.sbsr.2021.100415).
- [31] D. Routkevitch, T. Bigioni, M. Moskovits, and J. M. Xu, "Electrochemical fabrication of CdS nanowire arrays in porous anodic aluminum oxide templates," *J. Phys. Chem.*, vol. 100, no. 33, pp. 14037–14047, Jan. 1996, doi: [10.1021/jp952910m](https://doi.org/10.1021/jp952910m).
- [32] X. Lu *et al.*, "US CDC real-time reverse transcription PCR panel for detection of severe acute respiratory syndrome coronavirus 2," *Emerg. Infectious Diseases*, vol. 26, no. 8, pp. 1654–1665, Aug. 2020, doi: [10.3201/eid2608.201246](https://doi.org/10.3201/eid2608.201246).
- [33] A. Wozniak *et al.*, "A simple RNA preparation method for SARS-CoV-2 detection by RT-qPCR," *Sci. Rep.*, vol. 10, no. 1, Oct. 2020, Art. no. 16608, doi: [10.1038/s41598-020-73616-w](https://doi.org/10.1038/s41598-020-73616-w).
- [34] T. G. W. Graham, C. Dugast-Darzacq, G. M. Dailey, X. Darzacq, and R. Tjian, "Simple, inexpensive RNA isolation and one-step RT-qPCR methods for SARS-CoV-2 detection and general use," *Current Protocols*, vol. 1, no. 4, Apr. 2021, Art. no. e130, doi: [10.1002/cpz1.130](https://doi.org/10.1002/cpz1.130).
- [35] Z. Zhao, H. Cui, W. Song, X. Ru, W. Zhou, and X. Yu, "A simple magnetic nanoparticles-based viral RNA extraction method for efficient detection of SARS-CoV-2," *BioRxiv*, Feb. 2020.
- [36] P. Gong, G. M. Harbers, and D. W. Grainger, "Multi-technique comparison of immobilized and hybridized oligonucleotide surface density on commercial amine-reactive microarray slides," *Anal. Chem.*, vol. 78, no. 7, pp. 2342–2351, Apr. 2006, doi: [10.1021/ac051812m](https://doi.org/10.1021/ac051812m).
- [37] D. Gillespie and S. Spiegelman, "A quantitative assay for DNA–RNA hybrids with DNA immobilized on a membrane," *J. Mol. Biol.*, vol. 12, no. 3, pp. 829–842, Jul. 1965, doi: [10.1016/S0022-2836\(65\)80331-X](https://doi.org/10.1016/S0022-2836(65)80331-X).
- [38] X. Li, Y. He, T. Zhang, and L. Que, "Aluminum oxide nanostructure-based substrates for fluorescence enhancement," *Opt. Exp.*, vol. 20, no. 19, pp. 21272–21277, Sep. 2012, doi: [10.1364/OE.20.021272](https://doi.org/10.1364/OE.20.021272).
- [39] A. Dorfman, N. Kumar, and J. Hamm, "Highly sensitive biomolecular fluorescence detection using nanoscale ZnO platforms," *Langmuir*, vol. 22, no. 11, pp. 4890–4895, May 2006, doi: [10.1021/la053270+](https://doi.org/10.1021/la053270+).
- [40] P. T. Lin *et al.*, "Engineering broadband and anisotropic photoluminescence emission from rare earth doped tellurite thin film photonic crystals," *Opt. Exp.*, vol. 20, no. 3, pp. 2124–2135, Jan. 2012, doi: [10.1364/OE.20.002124](https://doi.org/10.1364/OE.20.002124).
- [41] P. T. Lin, W. A. Russin, A. Joshi-Imre, L. E. Ocola, and B. W. Wessels, "Investigation of the optical response of photonic crystal nanocavities in ferroelectric oxide thin film," *J. Opt.*, vol. 17, no. 10, Sep. 2015, Art. no. 105402, doi: [10.1088/2040-8978/17/10/105402](https://doi.org/10.1088/2040-8978/17/10/105402).
- [42] A. Yamaguchi *et al.*, "Self-assembly of a silica–surfactant nanocomposite in a porous alumina membrane," *Nature Mater.*, vol. 3, no. 5, pp. 337–341, May 2004, doi: [10.1038/nmat1107](https://doi.org/10.1038/nmat1107).
- [43] N. I. Kovtyukhova, T. E. Mallouk, and T. S. Mayer, "Templated surface Sol–Gel synthesis of SiO₂ nanotubes and SiO₂-insulated metal nanowires," *Adv. Mater.*, vol. 15, no. 10, pp. 780–785, May 2003, doi: [10.1002/adma.200304701](https://doi.org/10.1002/adma.200304701).
- [44] B. Winkler, "Modification of the surface characteristics of anodic alumina membranes using Sol–Gel precursor chemistry," *J. Membrane Sci.*, vol. 226, nos. 1–2, pp. 75–84, Dec. 2003, doi: [10.1016/j.memsci.2003.07.015](https://doi.org/10.1016/j.memsci.2003.07.015).
- [45] M. Zhu, M. Z. Lerum, and W. Chen, "How to prepare reproducible, homogeneous, and hydrolytically stable aminosilane-derived layers on silica," *Langmuir*, vol. 28, no. 1, pp. 416–423, Jan. 2012, doi: [10.1021/la203638g](https://doi.org/10.1021/la203638g).
- [46] D. E. Brunetti B, "About estimating the limit of detection by the signal to noise approach," *Pharmaceutica Analytica Acta*, vol. 6, no. 4, pp. 1–4, 2015, doi: [10.4172/2153-2435.1000355](https://doi.org/10.4172/2153-2435.1000355).